

MIT Open Access Articles

Diverse Chemiresistors Based upon Covalently Modified Multiwalled Carbon Nanotubes

The MIT Faculty has made this article openly available. **Please share** how this access benefits you. Your story matters.

Citation: Wang, Fei, and Timothy M. Swager. "Diverse Chemiresistors Based Upon Covalently Modified Multiwalled Carbon Nanotubes." *Journal of the American Chemical Society* 133.29 (2011): 11181–11193.

As Published: <http://dx.doi.org/10.1021/ja201860g>

Publisher: American Chemical Society (ACS)

Persistent URL: <http://hdl.handle.net/1721.1/74235>

Version: Author's final manuscript: final author's manuscript post peer review, without publisher's formatting or copy editing

Terms of Use: Article is made available in accordance with the publisher's policy and may be subject to US copyright law. Please refer to the publisher's site for terms of use.



**Diverse Chemiresistors Based Upon Covalently Modified
Multi-Walled Carbon Nanotubes**

Journal:	<i>Journal of the American Chemical Society</i>
Manuscript ID:	ja-2011-01860g.R1
Manuscript Type:	Article
Date Submitted by the Author:	n/a
Complete List of Authors:	Wang, Fei; Massachusetts Institute of Technology, Chemistry and Materials Science and Engineering Swager, Timothy; Mass. Inst. of Tech., Chemistry; Massachusetts Institute of Technology, Department of Chemistry 18-597

SCHOLARONE™
Manuscripts

Diverse Chemiresistors Based Upon Covalently Modified Multi-Walled Carbon Nanotubes

Fei Wang and Timothy M. Swager*

*Departments of Materials Science and Chemistry, Massachusetts Institute of Technology, Cambridge,
Massachusetts 02139*

e-mail address: tswager@mit.edu

Abstract:

A diverse array of multi-walled carbon nanotube (MWCNT) sensory materials have been synthesized and used to create sensors capable of identifying volatile organic compounds (VOCs) on the basis of their functional groups. Functionalized MWCNTs with a series of cross-sensitive recognition groups were successfully synthesized via zwitterionic and post-transformation synthetic procedures. The incorporated chemical functional groups on MWCNT surfaces introduced greatly increased sensitivity and selectivity to the targeted analytes. The distinct response pattern of each chemical was subjected to statistical treatments, which led to a clear separation and accurate identification of 100 % of the VOCs. These results demonstrate that covalent functionalized MWCNT-based sensor arrays are a promising approach for low-cost, real time detection and identification of VOCs.

Introduction

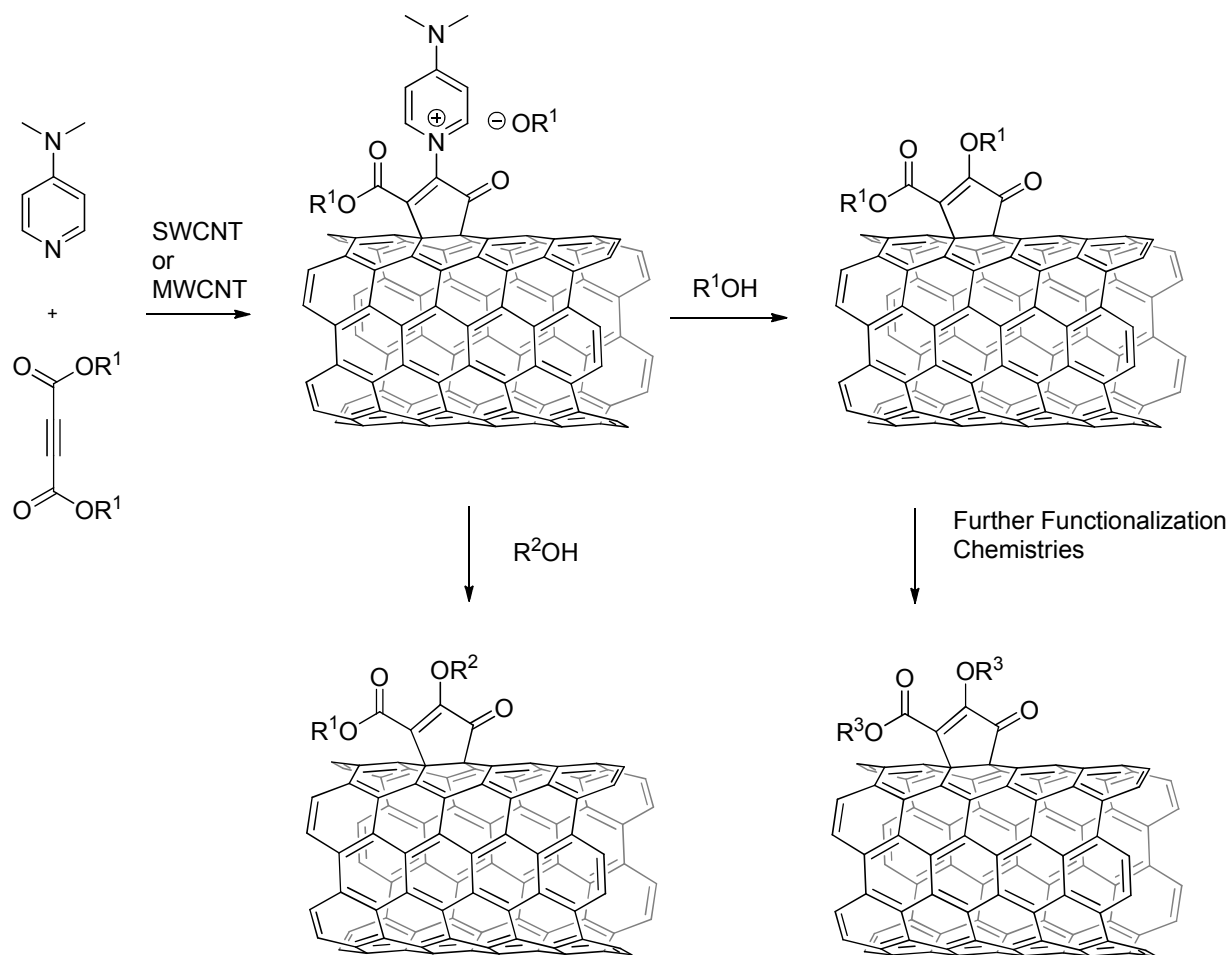
Real-time, sensitive detection and identification of volatile organic compounds are critically important to environmental monitoring and to human health. Widely used in many industries, many volatile organic chemicals (VOCs) can be toxic or carcinogenic even at relatively low concentrations. Additionally, VOCs in exhaled human breath have long been associated with certain diseases, and their detection and analysis have attracted a considerable

1
2
3 amount of scientific interest.¹ For example, hydrocarbons detected in a patient's exhaled
4 breath have been associated with cancer.^{2,3} Similarly, acetone is associated with uncontrolled
5 diabetes,⁴ isoprene with cholesterol metabolism disorders,^{5,6} and sulfur-containing compounds
6 with liver disfunctions.^{7,8} Breath analysis of exhaled VOCs have several obvious advantages
7 over traditional diagnostic techniques. It is non-invasive, sampling less complex sample
8 preparation than is required for blood or other body fluids, and has the potential for real-time
9 monitoring. However, one of the major limitations preventing breath analysis from being used
10 as a standard diagnostic technique is the lack of suitable and simple chemical detection and
11 identification techniques.¹ Present clinical vapor analysis methods include gas
12 chromatography-mass spectroscopy, solid-state metal oxide semiconductor sensors, and
13 electrochemical methods, all of which require bulky and/or expensive instruments as well as
14 considerable expertise to operate.⁹

15
16
17
18
19
20
21
22
23
24
25
26
27
28
29
30
31
32 Carbon nanotube (CNT)-based resistance-based chemical sensors have generated
33 tremendous interest over the past decade.¹⁰⁻¹³ Chemiresistors have the advantages of low
34 manufacturing cost, low power consumption, and minimal electronics. Additionally,
35 resistance-based sensors can be easily miniaturized and thereby incorporated into other systems.
36 Single-walled carbon nanotube (SWCNT) sensors are recognized as ultra-sensitive gas sensors,
37 and have been studied for medical detection of organic vapors, including non-polar molecules
38 as cancer markers,^{14,15} carbon dioxide,¹⁶ and ethanol.¹⁷ The high sensitivity in SWCNT-based
39 sensors is a result of the fact that their conductance dramatically responds to different chemical
40 environments through charge transfer, charge carrier pinning, Schottky barrier changes, or
41 CNT network swelling.¹⁰⁻¹³ A recent simulation study indicated that the sensing response of
42 pristine nanotube networks is mainly induced by modulation of junction resistance, while the
43
44
45
46
47
48
49
50
51
52
53
54
55
56
57
58
59
60

1
2
3 response of highly defective nanotube networks was mainly modulated by change in the
4 nanotube resistance.¹⁸ As a result of the interest in maintaining relative high conductance,
5 selectivity is generally introduced into SWCNT-based sensors through non-covalent
6 modification as opposed to covalent sidewall functionalization. Specifically disruptions in the
7 π -system on the nanotube surface can give resistance increases by 3 orders of magnitude,¹⁹ and
8 differential functionalization leads to large batch to batch variance in conductance and an
9 increased background resistance that limits sensitivity. Although non-covalent
10 functionalization methods can generate selectivity, they generally do not result in sensors that
11 are sufficiently robust for harsh environment applications. With the goal of harnessing
12 covalent modification of CNT sidewalls as a means to create a diverse array of robust sensors,
13 we have decided to create chemiresistors having MWCNTs as the conductive element. The
14 reasons for picking MWCNTs is that the dominance of the functionalization will be restricted
15 to the outer most graphene wall and thereby the inner tubes will continue to be highly
16 conductive. As a result we envision a chemiresistor where the MWCNT nanowires are made
17 to have “functional insulation” about them and selective binding of analytes to the insulation
18 will cause changes in the bulk conductance by modifying the inter-nanotube resistance. In
19 addition, polymer-carbon black conductive composites have also been widely explored for
20 resistance based array sensing by swelling of the percolating network, and have achieved good
21 sensitivity and selectivity.^{20,21} In these systems the dispersion depends on the compatibility of
22 carbon black and the polymer matrix, and melt-mixing followed by extrusion can be required
23 to avoid excessive aggregation of carbon black.²² In contrast, our bottom-up approach uses
24 surface modification of MWCNTS, and room temperature solution processes provide stable
25 nanotube dispersions (“inks”) for device construction.
26
27
28
29
30
31
32
33
34
35
36
37
38
39
40
41
42
43
44
45
46
47
48
49
50
51
52
53
54
55
56
57
58
59
60

1
2
3 To install a range of surface bound functional groups we have made use of a recently
4 developed efficient modular functionalization method that can be applied to CNTs and
5 fullerenes.^{23,24} The key reaction is initiated by a zwitterionic complex between 4-
6 dimethylaminopyridine (DMAP) and disubstituted acetylenedicarboxylates (Scheme 1). The
7 functionalization density can be as high as one incorporated functional group per nine carbons
8 for SWCNTs and one per thirty-eight carbons for multi-walled CNTs (MWCNTs). This
9 approach allows for functionalization to create a diversity of sensory materials through
10 modular nucleophilic substitution reactions of added alcohols with reactive pyridinium
11 intermediates and transformations of reactive functional groups introduced by this method
12 (Scheme 1).
13
14
15
16
17
18
19
20
21
22
23
24
25
26
27
28
29
30
31
32
33
34
35
36
37
38
39
40
41
42
43
44
45
46
47
48
49
50
51
52
53
54
55
56
57
58
59
60



35
36
37
38
39
40
41

Scheme 1. Schematic representation of the reaction schemes for modular functionalization of CNTs. For clarity a SWCNT segment is shown with only a single added functional group.

42
43
44
45
46
47
48
49
50
51
52
53
54
55
56
57
58
59
60

In this contribution we report a proof-of-concept sensing scheme using covalently functionalized MWCNTs to provide clear classification of VOCs based on functional group identification. We functionalized MWCNTs with a series of molecular recognition elements with differential binding abilities via zwitterionic functionalization and post-transformation synthetic strategies. We demonstrate that the functionalized MWCNT sensor array has a dramatically enhanced sensing response to a variety of VOCs compared to pristine MWCNTs. The incorporation of molecular recognition elements has created a distinct response pattern for

each of the chemicals investigated. Principal component analysis and linear discriminant analysis of the sensing data yielded a clear separation of the VOCs by their chemical families.

Design of the Sensor Array

The methodology for the array sensing is summarized in Figure 1. Initially, we observe the real time response of sidewall modified MWCNT sensor elements to selected VOCs. The obtained responses are then subjected to statistical treatments according to which analytes are then identified. Compared with individual sensors, array sensors have the advantages of responding to a wider range of analytes, improving selectivity, and identifying rather than only detecting a particular analyte.^{25,21} Array sensing using multiple receptors and pattern recognition process is very similar to the mammalian olfactory system and such devices have been referred to as “electronic noses” or “e-noses”.

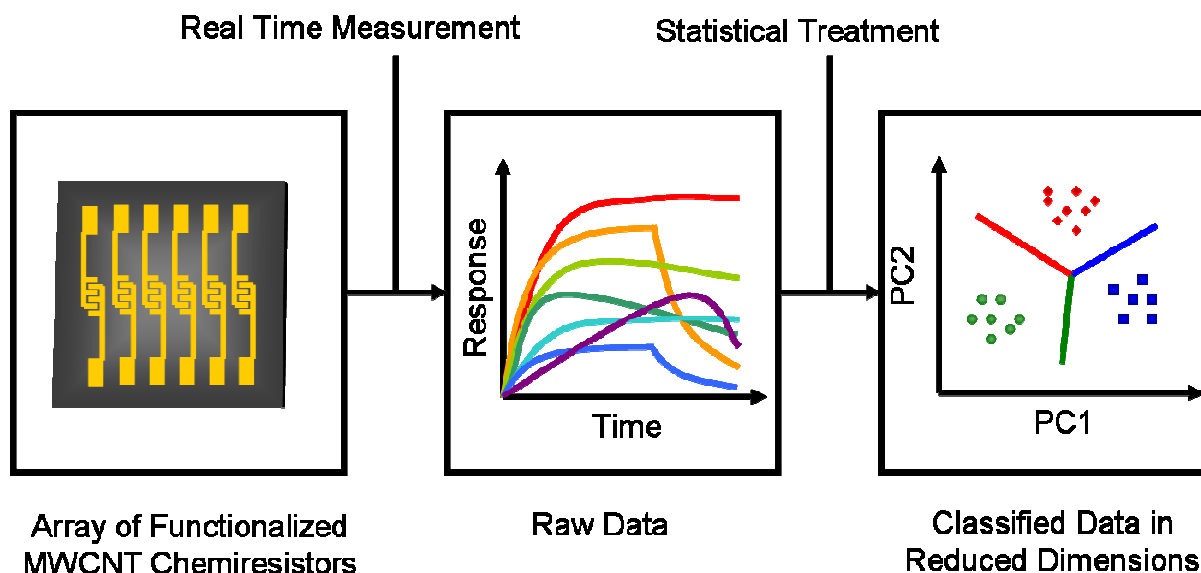


Figure 1. Outline of an array sensing process.

1
2
3 Table 1 summarizes twenty VOCs selected as the test analytes. Each analyte has
4 different chemical characteristics and different saturated vapor pressures. Unlike many highly
5 reactive toxic gases which can be selectively detected on the basis of their strong chemical
6 interactions such as Lewis acid-base, Brønsted acid-base or redox reactions, we chose to focus
7 on VOCs that are relatively inert and are in principle more difficult to detect and identify.²⁶ As
8 a proof of concept, we selectively detected them in order to demonstrate the advantages of
9 incorporating diverse receptors/functionality in a sensor array.
10
11
12
13
14
15
16
17
18
19
20
21
22
23
24
25
26
27
28
29
30
31
32
33
34
35
36
37
38
39
40
41
42
43
44
45
46
47
48
49
50
51
52
53
54
55
56
57
58
59
60

Table 1. Twenty selected VOCs and their vapor pressures^a at 298 K.

Analyte Family/ Functional Group	Analyte	Vapor Pressure	
		(mm Hg)	(ppm V)
Aliphatic Hydrocarbons	Dodecane	0.0977	128
	Decane	1.132	1489
	Octane	11.17	14697
Aromatic Hydrocarbons	1,3,5-Trimethylbenzene	0.9514	1251
	Xylenes	4.887	6430
	Toluene	22.35	29407
	Benzene	62	81578
Chlorinated Hydrocarbons	Chlorobenzene	9.774	12860
	1,2-Dichloroethane	60.9	80131
	Chloroform	152.9	201184
Ethers	Di- <i>n</i> -hexylether	0.06224	81
	Di- <i>n</i> -butylether	5.069	6669
	Dioxane	29.63	38986
Ketones	2-Decanone	0.269	353
	Cyclohexanone	2.766	3639
	Methylethylketone	68.88	90631
Alcohols	1-Octanol	0.06366	83
	1-Pentanol	1.545	2032
	1-Butanol	4.49	5907
	Ethanol	49.48	65105

^a Vapor pressures were obtained and calculated from *Yaws' Handbook of Antoine Coefficients for Vapor Pressure*,²⁷ or from the EPA's EPI software suite (<http://www.epa.gov/opptintr/exposure/docs/episuitedl.htm>) and should be taken as approximate only.

As detailed earlier, we chose MWCNTs as a chemiresistor material because, like SWCNTs, they can provide a rapid response to analytes, good reproducibility, and good reversibility. Additionally, the inner tubes in MWCNTs can maintain their electronic properties with high densities of covalent functionalization whereas similar modifications

1
2
3 destroy the electronic structure of SWCNTs.²⁸ An additional issue with SWCNTs is their
4
5 sensitivity to humidity changes.^{29,30}
6
7

8 The recognition groups in our sensor array are designed to provide a variety of non-
9
10 covalent interactions with the VOCs' functional groups. Grate has developed a linear solvation
11
12 energy relationship (LSER) approach to quantify the VOC sorption with the contributing
13
14 interactions.³¹ These interactions include hydrogen bonding, dipole-dipole interactions,
15
16 polarizability, and hydrocarbon dispersion interactions. Figure 2 summarizes the strategic
17
18 design of recognition groups according to these interactions and targeted analytes for each case.
19
20 For hydrogen bonding we have employed the hexafluoroisopropanol (HFIP) group which can
21
22 maximize hydrogen bonding by its acidic hydroxyl group (*pKa* 9~10, similar to phenols).^{32,33}
23
24 We also included a carboxylic acid group in our sensors. Together these two groups are
25
26 targeted to hydrogen bond accepting vapors such as ethers and ketones. For hydrogen bonding
27
28 basicity, we selected a readily available amide and crown-ether group, which provides high
29
30 polarity and a pre-organized basic site. This element is targeted to interact with hydroxyl-
31
32 containing vapors such as alcohols and acids. The acetylenedicarboxylate ester adducts
33
34 obtained from the initial zwitterionic functionalization are both polar and hydrogen bond
35
36 accepting, and are thereby expected to interact strongly with vapors with large dipoles.
37
38 Calix[4]arenes have a highly polarizable pocket which favors the adsorption of aromatic and
39
40 chlorinated hydrocarbons. Long-chain dodecyl groups favor dispersion interactions (a balance
41
42 between the exoergic process and the endoergic cost by entropy change) with aliphatic
43
44 hydrocarbons.
45
46
47
48
49
50
51
52
53
54
55
56
57
58
59
60

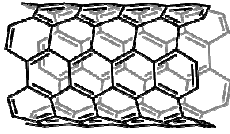
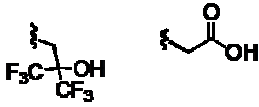
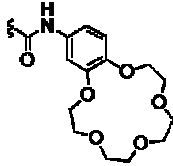
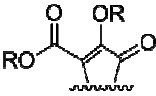
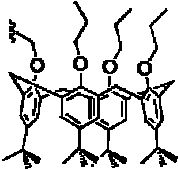

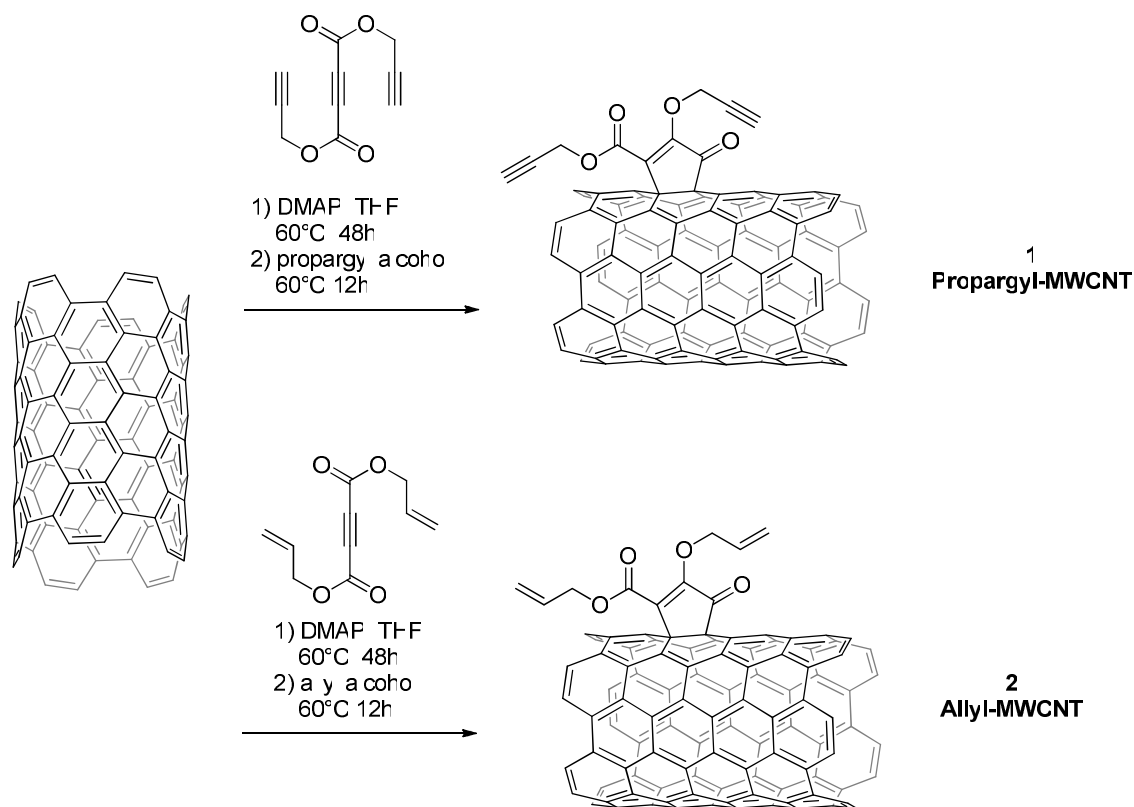
<p>MWCNT</p> 	<p>H-bond Acidity</p>  <p>Targeted Analytes: H-bond Acceptors such as Ethers, Ketones</p>	<p>H-bond Basicity</p>  <p>Targeted Analytes: H-bond Donors such as Acids, Alcohols</p>
<p>Polarity</p>  <p>R = allyl or propargyl</p> <p>Targeted Analytes: Vapors with High Polarity Such as Ketones, Ethers</p>	<p>Polarizability</p>  <p>Targeted Analytes: Aromatic and Chlorinated Hydrocarbons</p>	<p>Nonpolar Adsorption</p>  <p>Targeted Analytes: Aliphatic Hydrocarbons</p>

Figure 2. Selected recognition groups for differential interactions with targeted analytes.

Synthesis of Functionalized MWCNTs

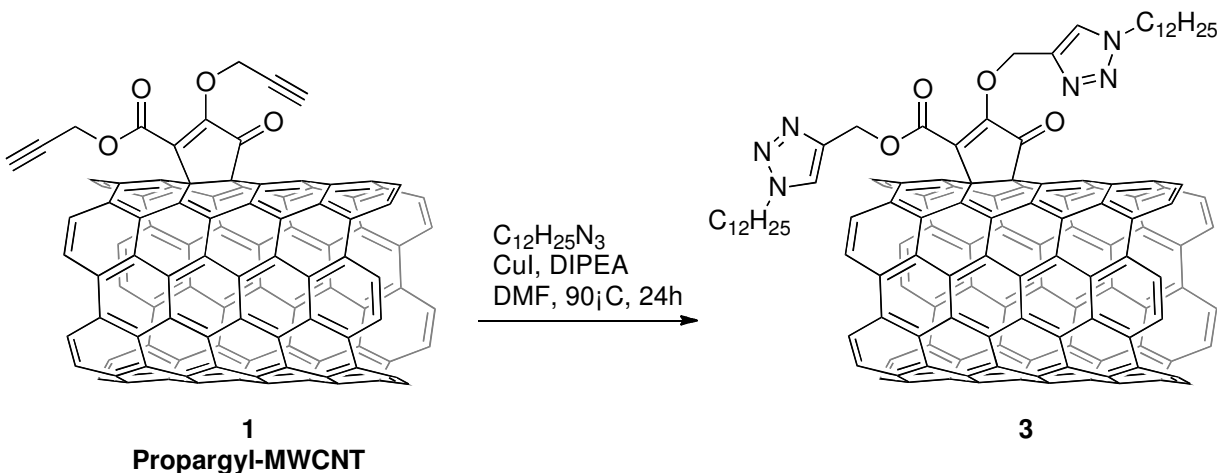
The syntheses of sidewall functionalized MWCNTs are summarized in Scheme 2-5. Propargyl or allyl groups were initially introduced on to MWCNTs under mild zwitterionic reaction conditions (THF, 60 °C) by first reacting with dipropargyl or diallyl acetylenedicarboxylate and DMAP, followed by the respective addition of excess propargyl- or allyl-alcohol to yield propargyl-MWCNT **1** and allyl-MWCNT **2** (Scheme 2).^{23,24}



32 **Scheme 2.** Synthesis of propargyl-MWCNT **1** and allyl-MWCNT **2**. Note the MWCNTs are
33 more complex polydisperse materials and for clarity a SWCNT segment is shown with only a
34 single added functional group.
35
36
37

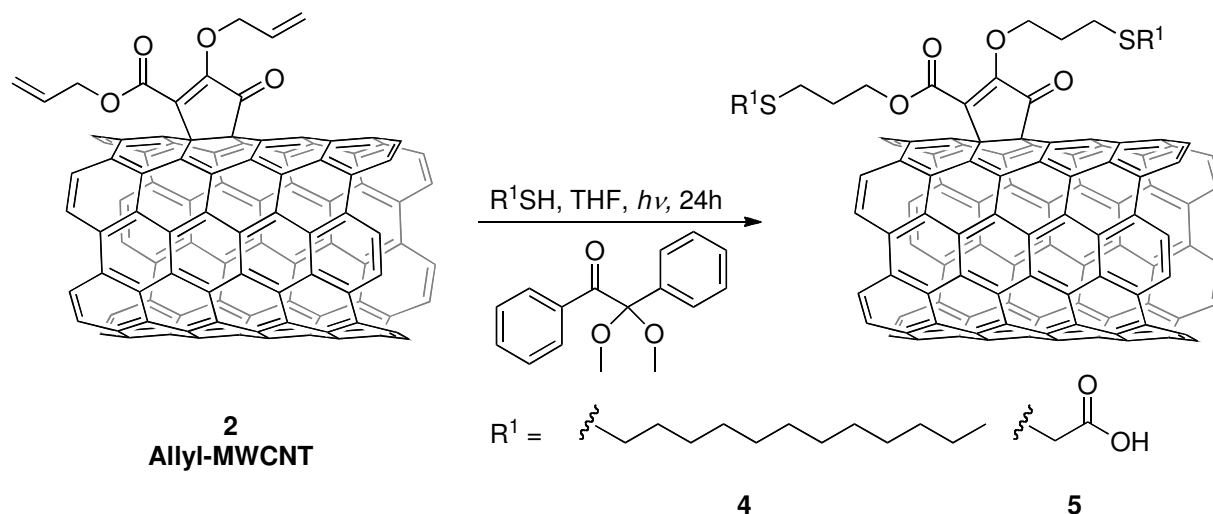
38
39
40
41 We have further functionalized **1** and **2** by three methods: 1,3-dipolar cycloaddition,
42 thiol-ene addition, and olefin cross-metathesis reactions. The 1,3-dipolar cycloaddition and
43 thiol-ene addition chemistry feature high yields and virtually no side products and are widely
44 utilized to modify polymers, nanoscale materials, and biological materials.^{34,35} Olefin
45 metathesis reactions, catalyzed by the Grubbs ruthenium catalysts, are another important route
46 to introduce diversity, as these reactions generally proceed in good yields and with high
47 functional group tolerance.^{36,37}
48
49
50
51
52
53
54
55
56
57
58
59
60

Using 1,3-dipolar cycloadditions dodecyl groups were incorporated onto the propargyl-MWCNTs **1** by reaction with dodecyl azide with CuI and diisopropylethylamine (DIPEA) as catalysts (Scheme 3). Heating this reaction mixture in DMF at 90 °C for 24h produced alkyltriazole-MWCNT **3** with pendant triazole groups.



Scheme 3. Synthesis of alkyltriazole-MWCNT **3**. Note the MWCNTs are more complex polydisperse materials and for clarity a SWCNT segment is shown with only a single added functional group.

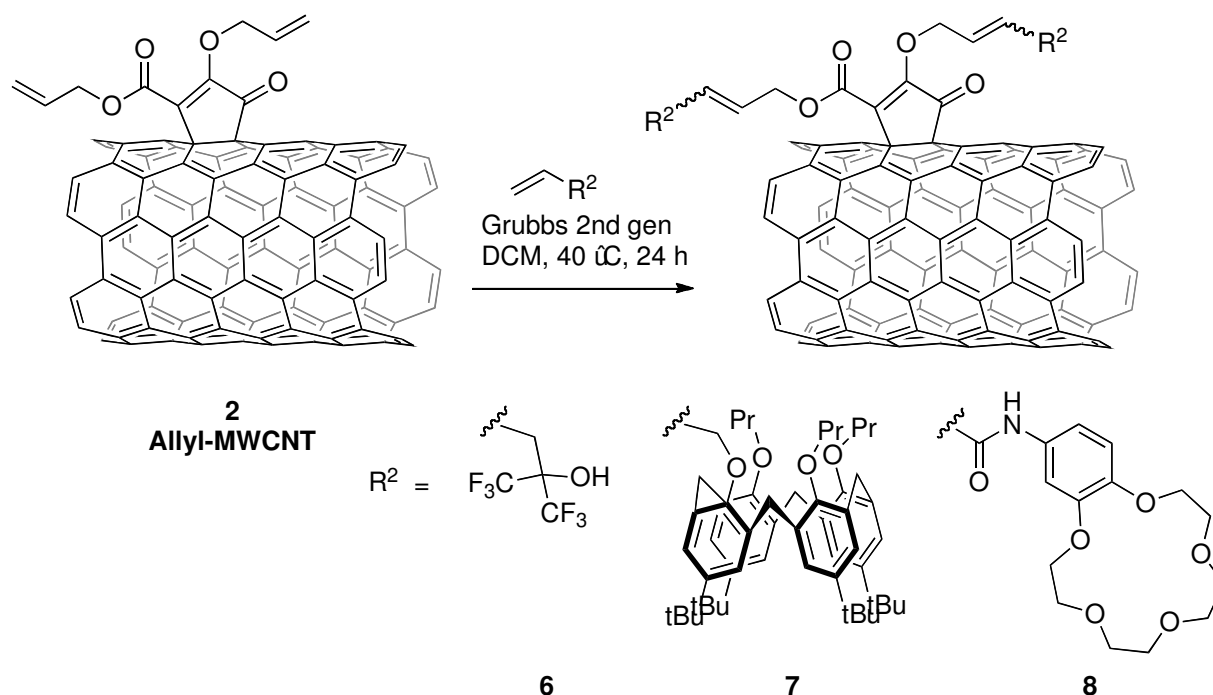
In the thiol-ene addition strategy, the vinyl group on allyl-MWCNT **2** was reacted with 1-dodecylthiol or thioglycolic acid under inert atmosphere with UV irradiation and 2,2-dimethoxy-2-phenylacetophenone as a photoinitiator (Scheme 4).^{35,38} These thiol-ene addition processes lead to the formation of thiochain-MWCNT **4** with pendant dodecyl chains and thioacid-MWCNT **5** with pendant carboxylic acid groups.



33
34
35
36
37
38
39
40
41
42
43
44
45
46
47
48
49
50
51
52
53
54
55
56
57
58
59
60

Scheme 4. Synthesis of thiochain-MWCNT **4** and thioacid-MWCNT **5**. Note the MWCNTs are more complex polydisperse materials and for clarity a SWCNT segment is shown with only a single added functional group.

Cross-metathesis reactions were conducted between the allyl-MWCNT **3** and three terminal olefins; 2-allyl-hexafluoroisopropanol, allyl substituted calix[4]arene, and 4-acryloylamidobenzo-15-crown-5, using Grubbs 2nd generation ruthenium catalyst,^{36,37} leading to HFIP-MWCNT **6**, calix-MWCNT **7** and crown-MWCNT **8**, respectively (Scheme 5).



Scheme 5. Synthesis of HFIP-MWCNT **6**, calix-MWCNT **7** and crown-MWCNT **8**. Note the MWCNTs are more complex polydisperse materials and for clarity a SWCNT segment is shown with only a single added functional group.

Characterization

Previous transmission electron microscopy (TEM) studies have revealed that the functionalization doesn't result in gross structural changes of the CNTs.²⁴ The Raman spectra of pristine MWCNTs, propargyl-MWCNTs **1** and allyl-MWCNTs **2** are compared in Figure 3. Two characteristic bands around 1330 cm^{-1} (D band) and 1580 cm^{-1} (G band) are immediately noticed. The D band reflects the structural disorder from defects or amorphous carbons, while the G band is associated with the tangential in-plane stretching vibration of the sp^2 carbon lattice. In contrast to SWCNTs, MWCNTs show an additional Raman band D' at around 1610 cm^{-1} , which is induced by disorder, defects, or ion intercalation between graphitic walls.^{39,40}

The three spectra could be fit with two Lorentzian peaks for the D and G bands, and with a Gaussian peak for the D' band.^{41,42} The ratio of the intensity between D and G band increased from 1.7 for pristine MWCNTs to 1.9 and 2.3 for propargyl-MWCNTs **1** and allyl-MWCNTs **2**, respectively; while the ratio of intensity between D' and G band remained the same (0.3) for all three samples. These results indicate that the zwitterionic functionalization reaction largely introduced covalent functionalization onto the MWCNT outer most graphene surface, with minimal perturbations to the inner tubes.

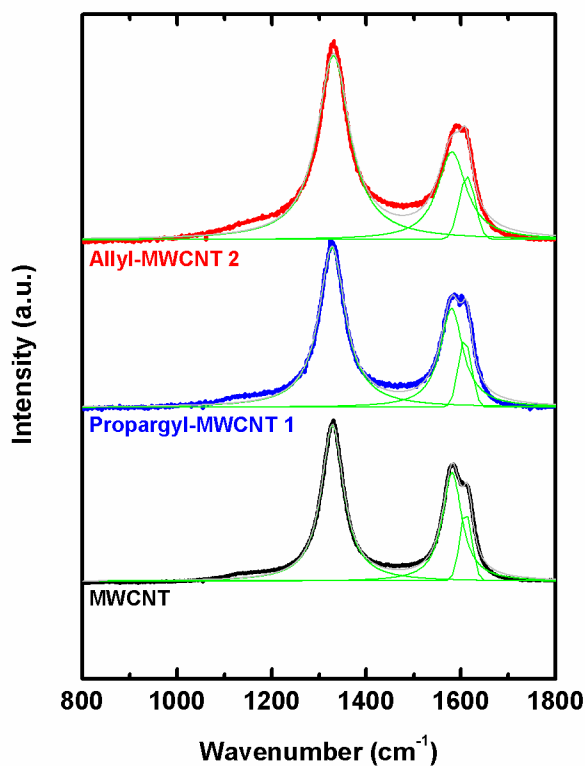


Figure 3. Raman spectra of pristine MWCNTs (black), propargyl-MWCNTs (blue) and allyl-MWCNTs (red). The green lines are fitted peaks and the grey lines are the fitted curves.

1
2
3
4
5
6
7
8
9
10
11
12
13
14
15
16
17
18
19
20
21
22
23
24
25
26
27
28
29
30
31
32
33
34
35
36
37
38
39
40
41
42
43
44
45
46
47
48
49
50
51
52
53
54
55
56
57
58
59
60

Although Raman spectroscopy gives evidence on the surface functionalization of nanotubes, Fourier transform infrared (FT-IR) spectroscopy reveals important chemical information regarding the incorporated functional groups.⁴³ As shown in Figure 4, all the functionalized MWCNTs have strong adsorption bands at 1730 cm⁻¹ due to the C=O stretching of the carbonyl group and bands at 1230 and 1020 cm⁻¹ assigned to the C-O stretching of the vinyl alkyl ether and ester groups. These features are consistent with the acetylenedicarboxylate diester adduct structure. All of the spectra of the functionalized MWCNTs were normalized according to the 1730 cm⁻¹ peak.

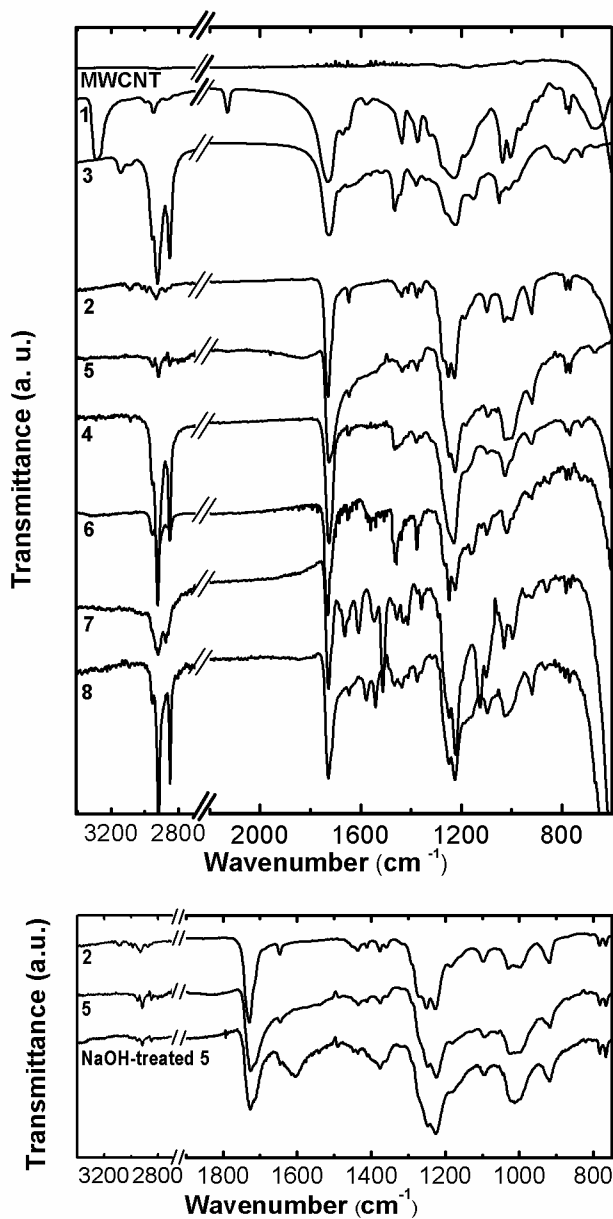


Figure 4. FT-IR spectroscopy of pristine and substituted MWCNTs (top): Propargyl-MWCNT **1**, allyl-MWCNT **2**, alkyltriazole-MWCNT **3**, thiochain-MWCNT **4**, thioacid-MWCNT **5**, HFIP-MWCNT **6**, calix-MWCNT **7**, and crown-MWCNT **8**. The spectra of thioacid-MWCNT treated with 0.1 M NaOH is also shown (bottom).

1
2
3 The propargyl-MWCNT **1** displays three characteristic absorption bands at 3285, 2130
4 and 668 cm^{-1} , corresponding to the terminal $\equiv\text{C}-\text{H}$ stretching, the $\text{C}\equiv\text{C}$ stretching and the
5 $\text{C}\equiv\text{C}-\text{H}$ bending of the propargyl group, respectively. After the 1,3-dipolar cycloaddition
6 reaction these three prominent bands completely disappear with concomitant enhanced peaks
7 within the 3000-2800 cm^{-1} region as a result of the $\text{C}-\text{H}$ stretching in the dodecyl groups, and
8 a new peak appearing at 3130 cm^{-1} associated with the $\text{C}-\text{H}$ stretching in the 1,2,3-triazole
9 groups. This result indicates that the 1,3-dipolar cycloaddition reaction proceeded in high yield
10 to produce **3**.
11
12
13
14
15
16
17
18
19
20
21

22
23 Allyl-MWCNT **2** showed characteristic absorption bands of vinyl groups at 3087 and
24 921 cm^{-1} , corresponding to the $=\text{CH}_2$ stretching and the CH_2 out-of-plane wagging,
25 respectively. After the thiol-ene addition, both bands of the allyl group had significantly
26 decreased compared to the $\text{C}=\text{O}$ stretching in the carbonyl group and the $\text{C}-\text{O}$ stretching bands,
27 indicating that the vinyl group has in large part undergone the proposed addition reaction.
28 Importantly, the thioacid-MWCNT **5** became soluble in 0.1M NaOH, and after base treatment
29 displayed two new broad peaks at 1605 and 1376 cm^{-1} , which are associated with the
30 asymmetric and symmetric stretching of the COO^- group, respectively (Figure 4, bottom). We
31 also observed greatly enhanced absorption between 3000 and 2800 cm^{-1} for thiochain-
32 MWCNTs **4**, which are due to the $\text{C}-\text{H}$ stretching in the dodecyl group. The large decrease of
33 the vinyl absorption peaks and the appearance of the characteristic IR peaks of the new
34 functional groups together verified the success of this thiol-ene addition modification.
35
36
37
38
39
40
41
42
43
44
45
46
47
48
49
50

51 Similar to the thiol-ene adducts, the MWCNTs from the metathesis reaction also
52 showed significantly decreased IR absorption signals from the vinyl group along with the
53 appearance of characteristic peaks of the new functional groups. Specifically, HFIP-MWCNT
54
55
56
57
58
59
60

1
2
3 6 showed a new peak at around 1170 cm^{-1} , corresponding to the C-F stretching in the HFIP
4 group. The crown-MWCNT 8 showed a series of interesting bands: two peaks at 1660 and
5
6 1548 cm^{-1} due to the C=O stretching and C-O stretching in the amide group, three peaks at
7
8 1610, 1510 and 1456 cm^{-1} due to the aromatic ring stretching of the benzene ring, and a peak at
9
10 1125 cm^{-1} due to the C-O-C three-centered stretching modes of the crown ether. The calix-
11
12 MWCNT 7 showed the appearance of two new peaks at 1580 and 1542 cm^{-1} due to the
13
14 aromatic ring stretching and a significant increase in the absorptions between 3000 and 2800
15
16 cm^{-1} due to the increased C-H stretching from the added *t*-butyl groups.
17
18
19
20
21

22 To obtain semi-quantitative assessment of the degree of functionalization and
23 composition of the modified MWCNTs we have employed X-ray photoelectron spectroscopy
24 (XPS) and thermogravimetric analysis (TGA). The XPS spectra (Figure 5) were normalized to
25 the C 1s peak at 532 eV. In the TGA experiment (Figure 6), pristine MWCNTs cleaned in the
26 same fashion as the functionalized MWCNTs were used as a standard. The weight loss data
27 are obtained from subtracting the weight loss of the pristine MWCNTs.
28
29
30
31
32
33
34
35
36
37
38
39
40
41
42
43
44
45
46
47
48
49
50
51
52
53
54
55
56
57
58
59
60

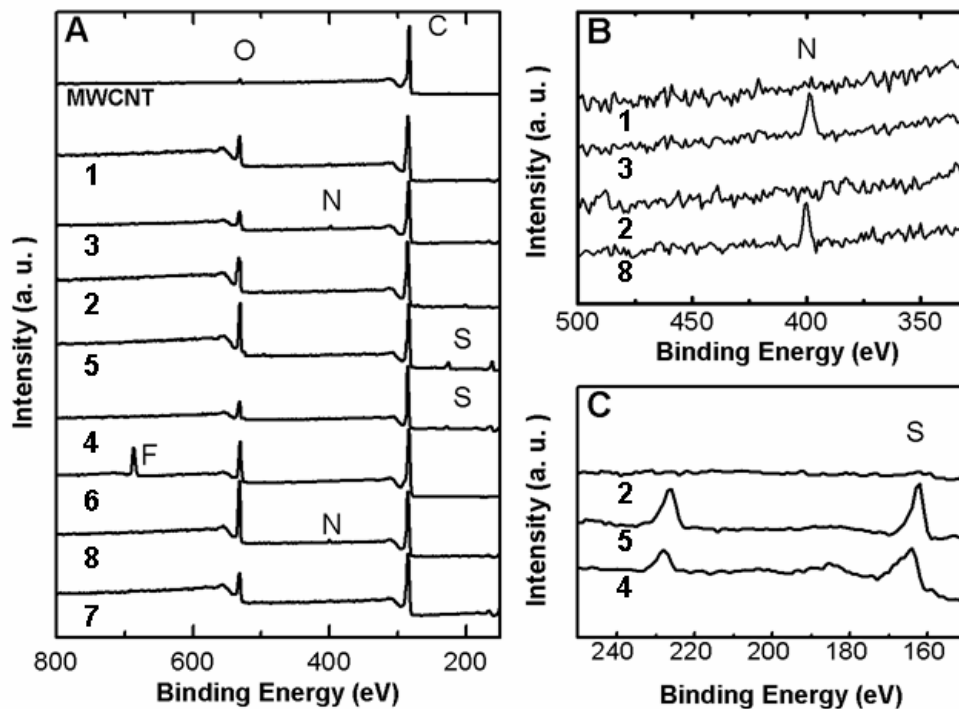


Figure 5. XPS of pristine and substituted MWCNTs: Propargyl-MWCNT **1**, allyl-MWCNT **2**, alkyltriazole-MWCNT **3**, thiochain-MWCNT **4**, thioacid-MWCNT **5**, HFIP-MWCNT **6**, calix-MWCNT **7**, and crown-MWCNT **8**. (A) Broad scans showing relevant F, O, N and S peaks. (B) Expanded view of the N peaks. (C) Expanded view of the S peaks.

Compared to pristine MWCNTs, both propargyl-MWCNTs **1** and allyl-MWCNTs **2** have increased intensity of oxygen 1s peak at 284 eV, indicating the success of the functionalization. From the oxygen-to-carbon ratio (7 %), the calculated degree of functionalization density for propargyl-MWCNT **1** is 2 propargyl diester adduct groups per 100 MWCNT carbon atoms. This result agrees with the functionalization density of 2.0 functional groups per 100 MWCNT carbon atoms calculated from the weight loss of 24 % observed by TGA. Similar calculations were carried out for the allyl-MWCNTs **2**, leading to a

density of 3 allyl diester adduct groups per 100 MWCNT carbon atoms by XPS (oxygen-carbon ratio of 8 %) and 2.6 functional groups by TGA (weight loss of 29 %).

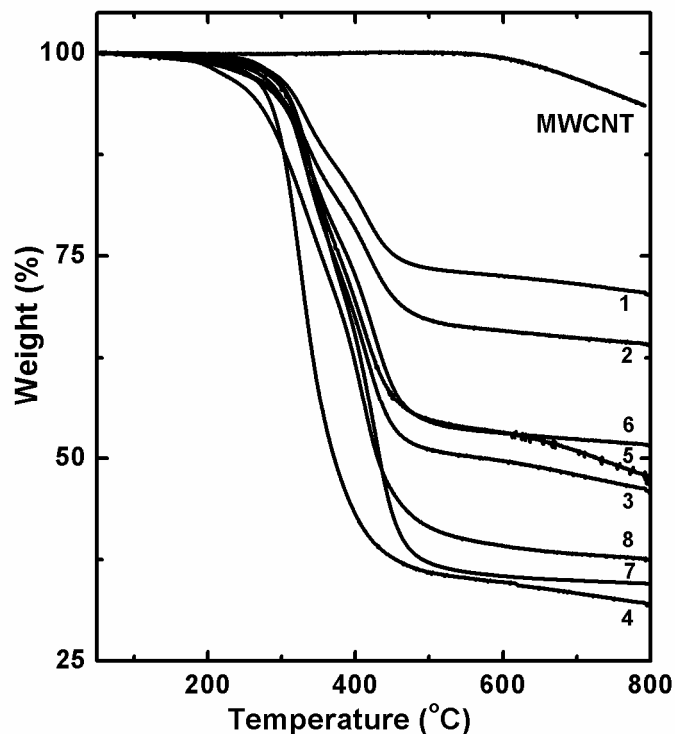


Figure 6. TGA of pristine and substituted MWCNTs: Propargyl-MWCNT **1**, allyl-MWCNT **2**, alkyltriazole-MWCNT **3**, thiochain-MWCNT **4**, thioacid-MWCNT **5**, HFIP-MWCNT **6**, calix-MWCNT **7**, and crown-MWCNT **8**.

We observed a distinct nitrogen 1s peak at 400 eV in the alkyltriazole-MWCNT **3** sample, and calculated the functionalization density of the triazole group from the oxygen-carbon ratio (5 %) or from the nitrogen-carbon ratio (6 %). These ratios corresponded to 4 triazole groups per 100 MWCNT carbon atoms. The weight loss of 48 % obtained from TGA measurements is in agreement and suggests functionalization density of 3.7 triazole groups per

100 carbon atoms. This high functionalization density indicated that the 1,3-dipolar cycloaddition chemistry is effectively quantitative on propargyl-MWCNTs **1**, which was consistent with our FT-IR observations.

Important information on the elemental composition of other samples was also obtained from XPS. We noticed that the functionalization reaction led to quite different oxygen-nitrogen ratios in each sample. We also observed sulfur 2s and 2p peaks (at 229 and 165 eV, respectively) in thioacid-MWCNTs **5** and thiochain-MWCNTs **4**, a fluorine 1s peak at 687 eV in HFIP-MWCNTs **6**, and a nitrogen 1s peak at 400 eV in crown-MWCNTs **8**. Table 2 summarizes the functionalization density data calculated from the XPS elemental ratio and from the TGA curves.

Table 2. Functionalization Density Data Calculated from the XPS Elemental Ratio and from the TGA Weight Loss Curves.

Samples	XPS Elemental Ratio (%)		TGA Weight Loss (%)	Density (Numbers of Functional Groups per 100 Carbons)	
	O/C	X/C ^a		by XPS	by TGA
	Propargyl-MWCNT	7	-	24	2
Allyl-MWCNT	8	-	39	3	2.6
Alkyltriazole-MWCNT	5	6	48	4	3.7
Thiochain-MWCNT	6	3	62	5	5.6
Thioacid-MWCNT	15	3	45	4	4.6
HFIP-MWCNT	12	7	42	2	1.6
Calix-MWCNT	8	-	59	- ^b	1.3
Crown-MWCNT	17	2	56	2	3.1

^a X stands for the respective amount of nitrogen, sulfur or fluorine in the samples. ^b XPS data is not used for calculation because functional group has similar oxygen-carbon ratio to parent allyl-MWCNT.

Morphology and Dispersibility

The scanning electron microscope (SEM) images of functionalized MWCNTs are shown in Figure 7. As a comparison, pristine MWCNT were ultra-sonicated and cleaned in the same fashion as the functionalized MWCNTs and were used as a standard, ruling out the effect of ultra-sonication and solvent washing. Analysis of these images confirmed that the functionalization process greatly reduced the size of the bundles of pristine MWCNTs.

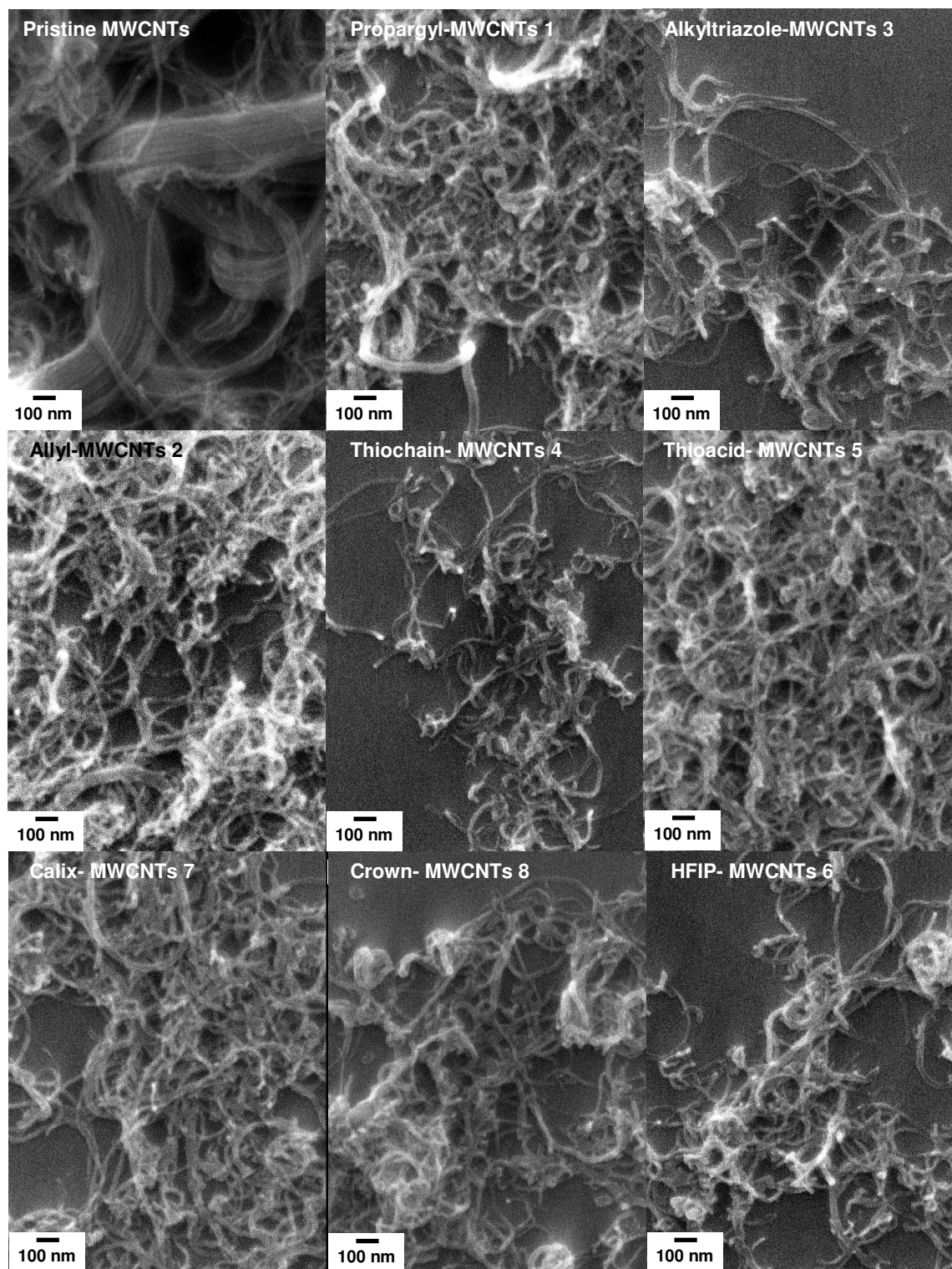


Figure 7. SEM images of pristine and substituted MWCNTs. The silicon substrates were cleaned by sonication in acetone/isopropanol/water successively and followed by cleaning with

1
2
3 oxygen plasma for 3 min. MWCNT dispersions (0.1 mg/mL) were spin-coated on top of the
4 substrates, and then annealed under vacuum at 150 °C for 5 min.
5
6
7
8

9
10 Chemical treatment greatly enhanced the dispersibility of MWCNTs. For example,
11 after centrifuging thiochain-MWCNT **4** suspension in dichloromethane at 14.5 K rpm for 5
12 minutes, the vast majority of the material still remained in the supernatant layer. Untreated
13 MWCNTs are quantitatively precipitated with similar treatment. This increase in dispersibility
14 is not surprising, given the high density of long dodecyl chains (5.6 dodecyl groups per 100
15 MWCNT carbon atoms by TGA), and the debundled nature of the functionalized MWCNTs.
16 Similar stable dispersibility was also found with the HFIP-MWCNTs **6** and the thioacid-
17 MWCNTs **5** in tetrahydrofuran, the crown-MWCNTs **8** in isopropanol, the calix-MWCNTs **7**,
18 and the alkyltriazole-MWCNTs **3** in dichloromethane. These good dispersion properties
19 enable us to achieve high-quality CNT conductive networks, which are critical for sensor
20 fabrication.
21
22
23
24
25
26
27
28
29
30
31
32
33
34
35
36
37

38 **Sensory Responses of Functionalized MWCNTs to VOCs**

39
40 We fabricated our chemiresistors by spin coating dispersions (0.1 mg/mL) of
41 functionalized MWCNTs on to 2 mm x 2 mm pairs of gold electrodes (50 nm thick, 2 mm
42 spacing) on glass substrates. The solvents with the best dispersing ability, as mentioned in the
43 morphology section, were used to create the solutions for spin coating of functionalized
44 MWCNTs. Dimethylformamide was used for dispersing pristine, allyl- and propargyl-
45 MWCNTs. The sensors were annealed after spin coating in vacuum at 150 °C for 5 minutes
46 before obtaining measurements. The typical thickness of the MWCNT films was in the range
47
48
49
50
51
52
53
54
55
56
57
58
59
60

1
2
3 of 30-60 nm measured with a profiler. The initial resistances for the MWCNT chemiresistors
4
5 were in the range of 0.2 to 0.5 M Ω .
6
7

8 We investigated the sensory response by measuring the relative conductance change
9
10 ($-\Delta G/G_0$) of the sensors upon exposure to the 20 VOCs at 1% of their saturated vapor
11
12 pressures (3 trials each). The current was recorded between two electrodes under a constant
13
14 bias voltage (0.05 V) from which the conductance change was calculated. Each sensor's
15
16 response was measured sequentially under the same experimental conditions such as sensor
17
18 exposure and refreshing time, analyte concentration, temperature, environmental humidity, *etc.*
19
20
21
22

23 Representative response curves of the sensor elements (pristine-MWCNTs, allyl-
24
25 MWCNT **2**, thiochain-MWCNTs **4** and crown-MWCNTs **8**) to 1% saturated vapors of decane
26
27 (left) and pentanol (right) are shown in Figure 8. All the sensors responded to the analyte very
28
29 rapidly and the chemical functionalization enhanced the response to both decane and pentanol.
30
31 It is interesting that the conductance of the thiochain-MWCNTs **4** and the crown-MWCNTs **8**
32
33 chemiresistors displayed complementary responses to decane and pentanol. This cross-
34
35 sensitivity reflects the different chemical properties of the sensing elements. The long aliphatic
36
37 hydrocarbon chains in the thiochain-MWCNTs lead to a stronger interaction with aliphatic
38
39 hydrocarbons, and the amide and the crown ether groups in the crown-MWCNTs introduced
40
41 favorable hydrogen bonding interactions with alcohol functionality of the pentanol.
42
43
44
45
46
47
48
49
50
51
52
53
54
55
56
57
58
59
60

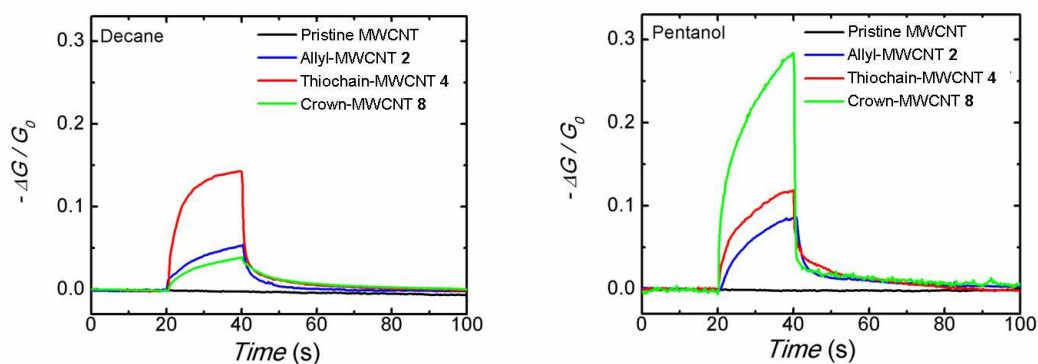


Figure 8. Conductance response, $-\Delta G/G_0$, of pristine MWCNTs (black line), allyl-MWCNTs 2 (dark red line), crown-MWCNTs 8 (green line), and thiochain-MWCNTs 4 (red line) resistance sensors to decane (left) and pentanol (right) at 1% of their saturated vapor pressures.

Figure 9 is the conductance response matrix of pristine and substituted MWCNT based resistance sensors to twenty representative VOCs (1% of their saturated vapor pressure). Each response is the average of three measurements. For easier visualization, the level of response is shown in color according to the scale bar on the right. The responses to each analyte are summarized in Figure S1 (supporting information), with excellent device-to-device repeatability. As expected from our chosen functionality, each of the VOCs induced different conductance changes in the individual sensors, thereby creating a unique multi-dimensional response pattern. Compared with pristine MWCNTs, functionalized MWCNTs have dramatically enhanced responses to all the VOCs. This sensitivity is attributed to the enhanced absorption of analytes to the functionalized nanotube surface and the largely debundled CNT network. As opposed to SWCNTs, MWCNTs have multiple graphenic layers and the electronic properties of the inner tubes are largely unaffected by surrounding chemical environment. The major mechanism of our MWCNT based sensor is, therefore, attributed to

the adsorption of analytes onto the exterior surfaces of the MWCNT network and the subsequent change of the inter-tube (junction) resistance. This mechanism is similar to that of polymer/carbon-black network. The difference between this MWCNT network and carbon black network is that our MWCNT sensor is based on molecular level dispersion/modification of surfaces, while carbon black conductive network is based on macroscale dispersion.

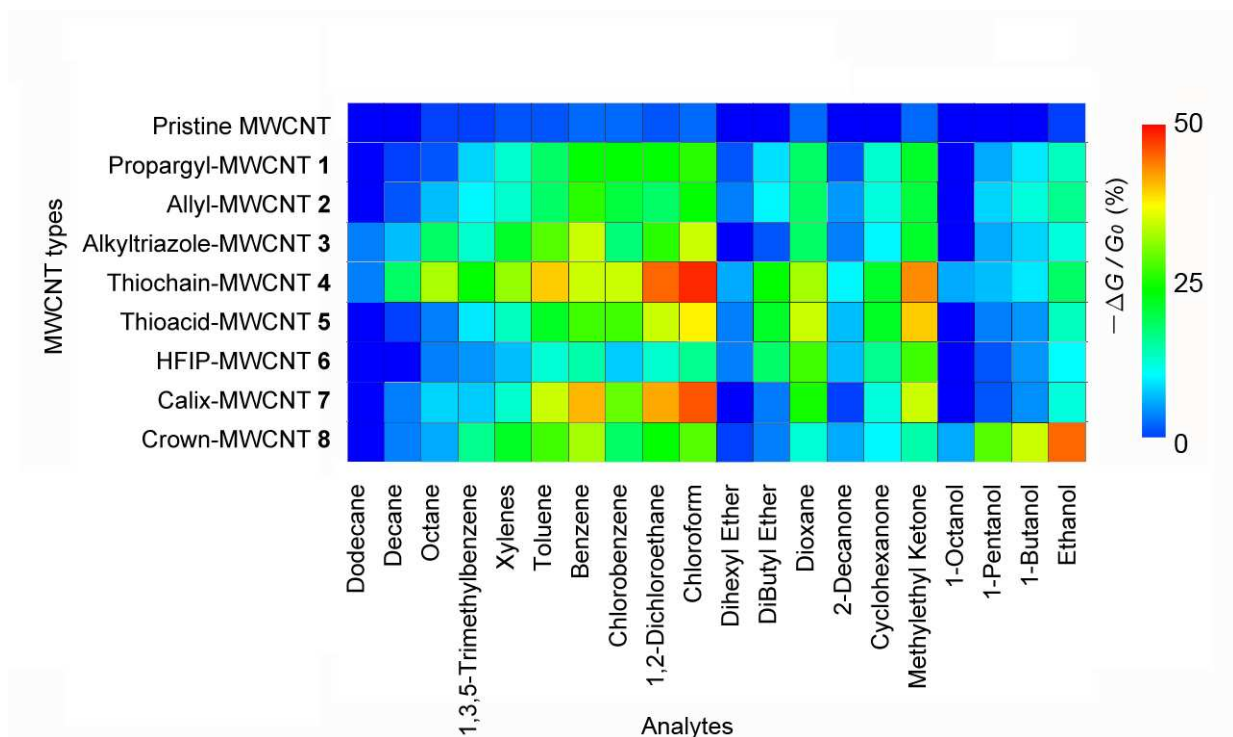


Figure 9. Conductance response patterns of pristine and substituted MWCNT based resistance sensors to twenty representative VOCs at 1% of their saturated vapor pressures. Responses are averages of three measurements. For easier visualization, the level of response is showed in color according to the scale bar on the right.

Simple inspection of the data yields examples of the expected selectivity. For example, the HFIP-MWCNT 6 sensor has an increased response to ethers and ketones as a consequence of the high hydrogen bonding acidity of the HFIP group. More interestingly, the HFIP-

1
2
3 MWCNT **6** sensor also showed a decreased response to all other VOCs. This latter property is
4 attributed to the non-favorable interactions between the HFIP's fluorocarbon groups and the
5 hydrocarbon-containing VOCs. As a second example, the thiochain-MWCNT **4** sensor had a
6 larger response to hydrocarbons with relatively low polarity such as aliphatic, aromatic and
7 chlorinated hydrocarbons. This is most likely due to the favorable dispersion interactions with
8 the aliphatic recognition groups. Similar responses were observed for alkyltriazole-MWCNTs
9
10
11
12
13
14
15
16
17
18 **3.** We noticed the enhanced responses of thiochain-MWCNTs **4** to almost all of the VOCs,
19 which is possibly due to its very high functionalization density (5.6 dodecyl groups per 100
20 MWCNT carbon atoms by TGA).
21
22
23
24
25
26

27 **Statistical Analysis**

28
29 To explore the capabilities of our sensor array to identify specific vapors, we subjected
30 our sensing results to principal component analysis and linear discriminate analysis. Principal
31 component analysis (PCA) is an unsupervised multivariate analysis method for linear data
32 compression and pattern recognition.⁴⁴ Without any prior knowledge of the classification of the
33 analytes, it groups the analytes based on the similarity of their data. The idea of PCA is to find
34 uncorrelated principle components (PCs), which are linear combinations of the original
35 variables (correlated response measurements). These PCs are ranked by the amount of
36 variation they account for. As shown in the Scree plot (Figure 10), the PCA of our data set
37 requires 2 PCs to describe 86 % of the total variances and 4 PCs to describe 95 % of the total
38 variances. The PCA score plot in Figure 11 shows a clear classification of the data, utilizing
39 the first two PCs, which represent 86 % of the variances. The VOCs were classified into five
40 groups, namely alcohols, ethers/ketones, aliphatic, aromatic, and chlorinated hydrocarbons.
41
42
43
44
45
46
47
48
49
50
51
52
53
54
55
56
57
58
59
60

The fact that both octanol and dihexyl ether have long aliphatic chains explains why their results also border the aliphatic hydrocarbon group. Although the ethers and the ketones are very clearly separated from other VOCs, it is difficult to distinguish them from each other because of their similar chemical properties.

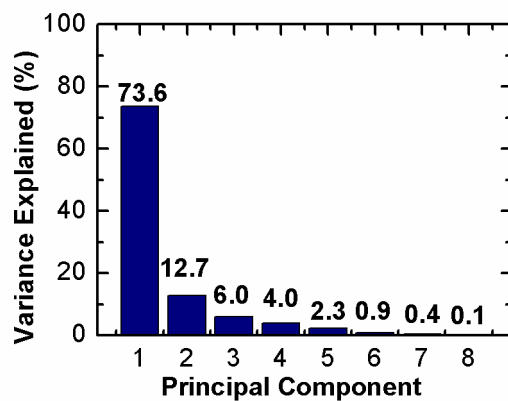


Figure 10. Scree plot of the principal component analysis.

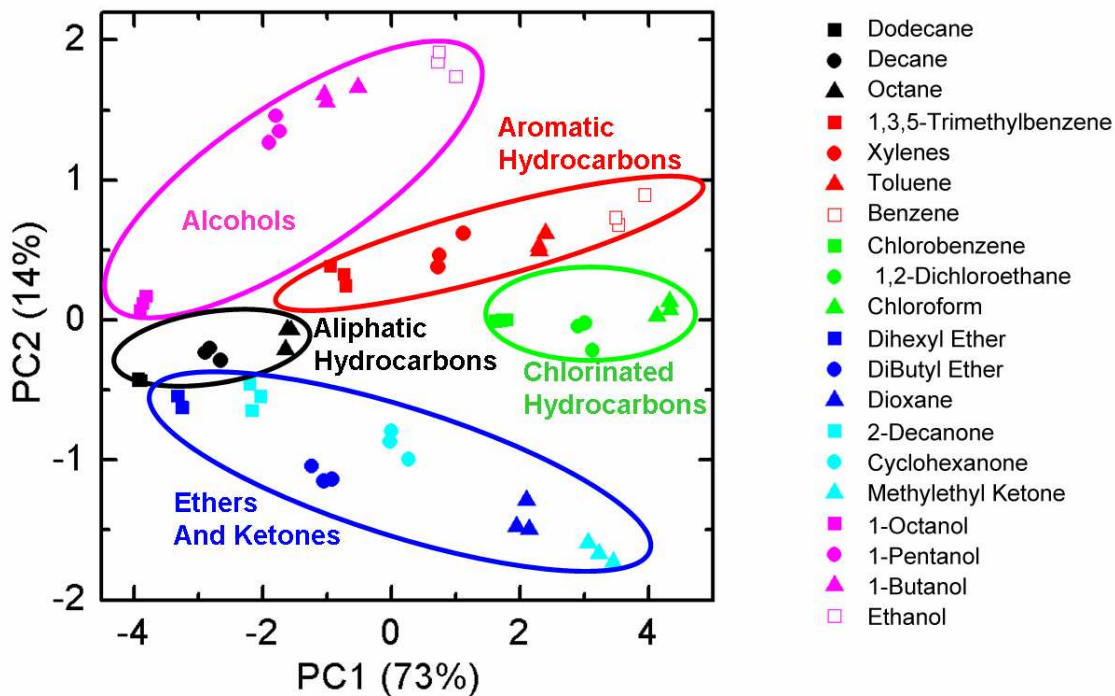


Figure 11. Principal component score plots of an array of 8 functionalized MWCNT resistance sensors to 20 representative VOCs (3 trials each).

We also explored the discrimination capability of our sensor with linear discriminant analysis (LDA).⁴⁴ LDA is a supervised statistical technique which utilizes data from known groups to identify which group a new object belongs to. It is based on the linear discriminant function (LDF), which is a linear combination of the original variables that maximizes the ratio of between-class variance and within-class variance. Specifically, we applied a cross-validation (leave-one-out) routine to compensate for an optimistic apparent error rate. This method calculates the LDF with one observation omitted sequentially and then classifies the omitted observation with the LDF. After this procedure is repeated for each observation the success rate is calculated. In our case, the 60 training observations (20 VOCs, 3 trials for each) were separated into the same 5 groups utilized in the PCA classification. As shown in Table 3, the cross-validation routine LDA demonstrated 100 % accuracy for all the 60 trials. This result, together with the successful PCA analysis, verified the excellent selectivity of our sensor array.

Table 3. Summary of Classification with Cross-validation.

Put-into-Group	True Group				
	Chlorinated Hydrocarbons	Ethers / Ketones	Aliphatic Hydrocarbons	Alcohols	Aromatic Hydrocarbons
Chlorinated Hydrocarbons	9	0	0	0	0
Ethers / Ketones	0	18	0	0	0
Aliphatic Hydrocarbons	0	0	9	0	0
Alcohols	0	0	0	12	0
Aromatic Hydrocarbons	0	0	0	0	9
Total N	9	18	9	12	9
N Correct	9	18	9	12	9

Proportion	1.00	1.00	1.00	1.00	1.00
N = 60	N Correct = 60		Proportion Correct = 1.000		

Humidity Response

Environmental humidity is always a concern for nanotube based sensors. As shown in Figure 12, our sensors have lower responses to humidity compared to their responses to organic molecules such as pentanol, although the saturated vapor pressure of water at 25 °C (23.8 mmHg) is 15 times larger than that of pentanol (1.5 mmHg). This fact can be explained by the hydrophobic nature of the incorporated chemical functionalizations. However, high humidity can potentially still generate relatively large responses when the MWCNTs are functionalized with strongly hydrogen bonding or Lewis acidic groups, or when the analyte concentration is very low. In this cases humidity corrections may be needed.

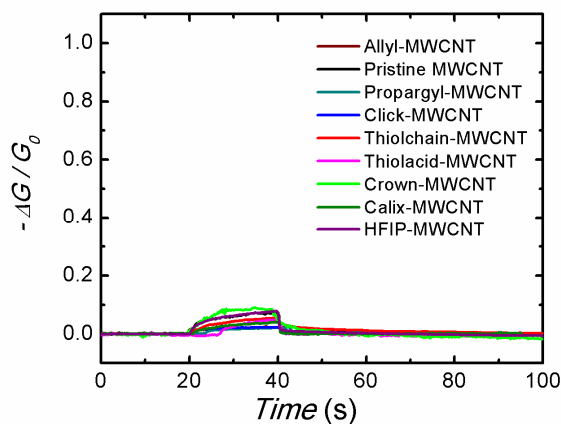


Figure 12. Conductance response, $-\Delta G/G_0$, of the pristine and substituted MWCNT based resistance sensors to saturated vapor of water.

3. Conclusions

1
2
3 Chemiresistor sensors capable of forming an array were developed from covalently
4
5
6 sidewall functionalized MWCNTs for identifying VOCs. Functionalized MWCNTs with a
7
8 series of cross-sensitive recognition groups were successfully synthesized via zwitterionic and
9
10 post-transformation synthetic approaches. The incorporated chemical functional groups on
11
12 MWCNT surfaces introduced greatly increased sensitivity and selectivity to the targeted
13
14 analytes. The covalent nature of the functionalization also yielded materials with excellent
15
16 stability. The distinct response pattern of each chemical was subjected to statistical treatments,
17
18 which led to a clear separation and accurate identification of 100 % of the VOCs. MWCNT-
19
20 based chemiresistive sensor arrays represent a promising approach for low-cost, real time
21
22 detection and identification of VOCs.
23
24
25
26
27
28

29 **Acknowledgement:** We are grateful for support from the National Science Foundation and
30
31 the Army Research Office through the Institute for Soldier Nanotechnologies.
32
33
34
35
36
37
38
39
40
41
42
43
44
45
46
47
48
49
50
51
52
53
54
55
56
57
58
59
60

4 Experimental Section

Materials.

All chemicals were of reagent grade from Sigma-Aldrich, Alfa Aesar or Acros and used as received. All solvents were of spectroscopic grade unless otherwise noted. Dimethylformamide was stirred over CaH₂ and distilled thereafter. Anhydrous tetrahydrofuran and dichloromethane were obtained from J. T. Baker and purified by passing through a Glasscontour dry solvent system. Multi-walled carbon nanotubes were acquired from Sigma-Aldrich. (> 99 MWCNT, O.D. 6-13 nm X 2.5-20 μm). Diallyl acetylenedicarboxylate and dipropargyl acetylenedicarboxylate were prepared according to literature procedures.²⁴ 5,11,17,23-Tetrakis(*t*-butyl)-25-allyl-26,27,28-tripropyl-calix[4]arene was prepared according to literature procedure.⁴⁵

General Methods and Instrumentation.

Raman spectra were measured with a Kaiser Hololab 5000R Modular Research Raman Spectrometer with Microprobe from MIT Center for Materials Science and Engineering. FT-IR spectra were recorded on a Perkin Elmer Model 2000 FT-IT spectrometer by drop-casting the material on a KBr disk. TGA analyses were performed with a TGA Q50 apparatus (TA instruments). Experiments were carried out under nitrogen. Samples were heated at 5 °C/min from 30 °C to 800 °C. XPS spectra were recorded on a Kratos AXIS Ultra X-ray Photoelectron Spectrometer. SEM images were taken with a JEOL 6700 Scanning Electron Microscope. Gold layer was coated from a Polaron SC7620 sputter coater. The substrates were cleaned with a Harrick Plasma PDC-32G Plasma Cleaner. Film thicknesses were measured with a Veeco Dektak 6M Stylus Profiler.

1
2
3 All synthetic manipulations were carried out under an argon atmosphere using standard
4 Schlenk techniques unless otherwise noted. Glassware was oven-baked and cooled under N₂
5 atmosphere. Analyte of specific concentration and relative humidity was generated with a
6 KIN-TEK gas-generating system. Source-drain current change in response to analyte was
7 measured with an AUTOLAB PGSTAT 20 potentiostat (Eco Chemie) at constant potential
8 (typically 0.05 V). The statistical treatment was performed with a Minitab software (version
9 15) using multivariate analysis methods.
10
11
12
13
14
15
16
17
18
19
20
21

22 **Synthesis of Propargyl-MWCNTs 1.**

23

24 A suspension of MWCNTs (48.0 mg, 4.0 mmol of carbon) in THF (40 mL) was
25 sonicated for 5 min using an ultrasonic probe yielding a black suspension. To the MWCNT
26 suspension were added activated molecular sieves (4 Å) to remove moisture introduced by the
27 sonication process, and left overnight. The heterogeneous solution was then transferred to a
28 dry flask through a cannula and was heated at 60 °C. To the MWCNT suspension were added
29 simultaneously a solution of dipropargyl acetylenedicarboxylate (3.80 g, 20.0 mmol) in THF
30 (20 mL) and a solution of 4-dimethylaminopyridine (2.44 g, 20.0 mmol) in THF (20 mL) via
31 syringe pump over 48h. Propargyl alcohol (1.5 mL) was then added and the resulting mixture
32 was stirred at 65 °C for another 12 h. The reaction mixture was cooled to room temperature,
33 and centrifuged at 14,500 rpm for 15 min. The supernatant was discarded and the residue was
34 dispersed in DMF for 3 min using an ultrasonic bath. The mixture was centrifuged and the
35 supernatant was discarded. The same dispersion, centrifugation, and supernatant separation
36 sequence was repeated five times with DMF and five times with acetone to remove impurities.
37
38
39
40
41
42
43
44
45
46
47
48
49
50
51
52
53
54
55
56
57
58
59
60

The propargyl-MWCNTs **1** were dried under vacuum overnight. See Figure 3 for Raman

1
2
3 spectra, Figure 4 for FT-IR spectra, Figure 5 for XPS spectra, Figure 6 for TGA weight loss
4
5
6 curve, and Figure 7 for SEM image.
7
8
9

10 **Synthesis of Allyl-MWCNTs 2.**

11
12 A suspension of MWCNTs (48.0 mg, 4.0 mmol of carbon) in THF (40 mL) was
13
14 sonicated for 5 min using an ultrasonic probe yielding a black suspension. To the MWCNT
15
16 suspension were added activated molecular sieves (4 Å) to remove moisture introduced by the
17
18 sonication process, and left overnight. The heterogeneous solution was then transferred to a
19
20 dry flask through a cannula and was heated at 60 °C. To the MWCNT suspension were added
21
22 simultaneously a solution of diallyl acetylenedicarboxylate (3.88 g, 20.0 mmol) in THF (20 mL)
23
24 and a solution of 4-dimethylaminopyridine (2.44 g, 20.0 mmol) in THF (20 mL) via syringe
25
26 pump over 48h. Allyl alcohol (1.5 mL) was then added, and the resulting mixture was stirred at
27
28 65 °C for another 12 h. The reaction mixture was cooled to room temperature, and centrifuged
29
30 at 14,500 rpm for 15 min. The supernatant was discarded and the residue was dispersed in
31
32 DMF for 3 min using an ultrasonic bath. The mixture was centrifuged and the supernatant was
33
34 discarded. The same dispersion, centrifugation, and supernatant separation sequence was
35
36 repeated five times with DMF and five times with acetone to remove impurities. The allyl-
37
38 MWCNTs **1** were dried under vacuum overnight. See Figure 4 for FT-IR spectra, Figure 5 for
39
40 XPS spectra, Figure 6 for TGA weight loss curve, and Figure 7 for SEM image.
41
42
43
44
45
46
47
48
49
50

51 **Synthesis of alkyltriazole-MWCNTs 3.**

52
53 To a 10 mL Schlenk flask was added propargyl-MWCNTs **1** (10 mg) and CuI (38 mg,
54
55 0.2 mmol), followed by sequentially vacuuming and refilling with argon three times. Then
56
57
58
59
60

1
2
3 dodecyl azide (0.22 g, 1 mmol), diisopropylethylamine (2 mL) and dimethylformamide (2 mL)
4
5 were added via syringe. The mixture was sonicated in a sonication bath for 30 min, followed
6
7 by stirring at 90 °C for 24 h. The reaction mixture was cooled to room temperature, and
8
9 washed with ammonium hydroxide for five times to remove copper. Interestingly, the
10
11 MWCNTs were well dispersed in the diisopropylethylamine phase during the washing process,
12
13 so a 25 mL separation funnel was used to collect the diisopropylethylamine phase. The
14
15 dispersion was further washed with water three times to remove residue ammonium hydroxide.
16
17 The dispersion was added to methanol and centrifuged at 14,500 rpm for 15 min. The
18
19 supernatant was discarded and the residue was dispersed in acetone for 3 min using an
20
21 ultrasonic bath. The mixture was centrifuged and the supernatant was discarded. The same
22
23 dispersion, centrifugation, and supernatant separation sequence was repeated five times with
24
25 acetone to remove impurities. The alkyltriazole-MWCNTs **3** were dried under vacuum
26
27 overnight. See Figure 3 for Raman spectra, Figure 4 for FT-IR spectra, Figure 5 for XPS
28
29 spectra, Figure 6 for TGA weight loss curve, and Figure 7 for SEM image.
30
31
32
33
34
35
36
37
38

39 **Synthesis of thiochain-MWCNTs 4.**

40
41 To a 10 mL Schlenk flask was added allyl-MWCNTs **2** (10 mg) and 2,2-dimethoxy-2-
42
43 phenylacetophenone (DMPA) (26 mg, 0.1 mmol), followed by sequentially vacuuming and
44
45 refilling with argon three times. Then *n*-dodecylthiol (0.40 g, 2 mmol) and tetrahydrofuran (2
46
47 mL) was added via syringe. The mixture was sonicated in a sonication bath for 30 min,
48
49 followed by stirring under UV irradiation at room temperature for 24 h. The reaction mixture
50
51 was then diluted with acetone and centrifuged at 14,500 rpm for 15 min. The supernatant was
52
53 discarded and the residue was dispersed in acetone for 3 min using an ultrasonic bath. The
54
55
56
57
58
59
60

1
2
3 mixture was centrifuged and the supernatant was discarded. The same dispersion,
4
5 centrifugation, and supernatant separation sequence was repeated five times with acetone to
6
7 remove impurities. The thiochain-MWCNTs **4** were dried under vacuum overnight. See
8
9 Figure 4 for FT-IR spectra, Figure 5 for XPS spectra, Figure 6 for TGA weight loss curve, and
10
11 Figure 7 for SEM image.
12
13
14
15
16
17

18 **Synthesis of thioacid-MWCNTs 5.**

19
20 To a 10 mL Schlenk flask was added allyl-MWCNTs **2** (10 mg) and 2,2-dimethoxy-2-
21
22 phenylacetophenone (DMPA) (26 mg, 0.1 mmol), followed by sequentially vacuuming and
23
24 refilling with argon three times. Then thioglycolic acid (0.18 g, 2 mmol) and tetrahydrofuran
25
26 (2 mL) was added via syringe. The mixture was sonicated in a sonication bath for 30 min,
27
28 followed by stirring under UV irradiation at room temperature for 24 h. The reaction mixture
29
30 was then diluted with acetone and centrifuged at 14,500 rpm for 15 min. The supernatant was
31
32 discarded and the residue was dispersed in acetone for 3 min using an ultrasonic bath. The
33
34 mixture was centrifuged and the supernatant was discarded. The same dispersion,
35
36 centrifugation, and supernatant separation sequence was repeated five times with acetone to
37
38 remove impurities. The thioacid-MWCNTs **5** were dried under vacuum overnight. See Figure
39
40 4 for FT-IR spectra, Figure 5 for XPS spectra, Figure 6 for TGA weight loss curve, and Figure
41
42 7 for SEM image.
43
44
45
46
47
48
49
50

51 **Synthesis of HFIP-MWCNTs 6.**

52
53 To a 10 mL Schlenk flask was added allyl-MWCNTs **2** (10 mg) and Grubbs second
54
55 generation ruthenium catalyst (8 mg, 0.01 mmol), followed by sequentially evacuating and
56
57
58
59
60

1
2
3 refilling with argon three times. Then 2-allyl-hexafluoroisopropanol (0.4 g, 2 mmol) and
4
5 dichloromethane (2 mL) was added via syringe. The mixture was sonicated in a sonication bath
6
7 for 30 min, followed by stirring at 40 °C for 48 h. The reaction mixture was then diluted with
8
9 acetone and centrifuged at 14,500 rpm for 15 min. The supernatant was discarded and the
10
11 residue was dispersed in acetone for 3 min using an ultrasonic bath. The mixture was
12
13 centrifuged and the supernatant was discarded. The same dispersion, centrifugation, and
14
15 supernatant separation sequence was repeated five times with acetone to remove impurities.
16
17
18 The HFIP-MWCNTs **6** were dried under vacuum overnight. See Figure 4 for FT-IR spectra,
19
20 Figure 5 for XPS spectra, Figure 6 for TGA weight loss curve, and Figure 7 for SEM image.
21
22
23
24
25
26

27 **Synthesis of Calix-MWCNTs 7.**

28
29 To a 10 mL Schlenk flask was added allyl-MWCNTs **2** (10 mg), Grubbs second
30
31 generation ruthenium catalyst (8 mg, 0.01 mmol) and 5,11,17,23-Tetrakis(*t*-butyl)-25-allyl-
32
33 26,27,28-tripropyl-calix[4]arene (0.16 g, 0.2 mmol) followed by sequentially evacuating and
34
35 refilling with argon three times. Then dichloromethane (2 mL) was added via syringe. The
36
37 mixture was sonicated in a sonication bath for 30 min, followed by stirring at 40 °C for 48 h.
38
39 The reaction mixture was then diluted with acetone and centrifuged at 14,500 rpm for 15 min.
40
41 The supernatant was discarded and the residue was dispersed in acetone for 3 min using an
42
43 ultrasonic bath. The mixture was centrifuged and the supernatant was discarded. The same
44
45 dispersion, centrifugation, and supernatant separation sequence was repeated five times with
46
47 acetone to remove impurities. The calix-MWCNTs **7** were dried under vacuum overnight. See
48
49 Figure 4 for FT-IR spectra, Figure 5 for XPS spectra, Figure 6 for TGA weight loss curve, and
50
51 Figure 7 for SEM image.
52
53
54
55
56
57
58
59
60

Synthesis of Crown-MWCNTs **8**.

To a 10 mL Schlenk flask was added allyl-MWCNTs **2** (10 mg), Grubbs second generation ruthenium catalyst (8 mg, 0.01 mmol) and 4-acryloylamidobenzo-15-crown-5 (0.14 g, 0.4 mmol) followed by sequentially evacuating and refilling with argon three times. Then dichloromethane (2 mL) was added via syringe. The mixture was sonicated in a sonication bath for 30 min, followed by stirring at 40 °C for 48 h. The reaction mixture was then diluted with acetone and centrifuged at 14,500 rpm for 15 min. The supernatant was discarded and the residue was dispersed in acetone for 3 min using an ultrasonic bath. The mixture was centrifuged and the supernatant was discarded. The same dispersion, centrifugation, and supernatant separation sequence was repeated five times with acetone to remove impurities. The crown-MWCNTs **8** were dried under vacuum overnight. See Figure 4 for FT-IR spectra, Figure 5 for XPS spectra, Figure 6 for TGA weight loss curve, and Figure 7 for SEM image.

Device Fabrication.

The glass substrates were cleaned by sonication in acetone/isopropanol/water successively and followed by cleaning with oxygen plasma for 5 min. Two gold strip electrodes (50 nm thick, 2 mm spacing) were sputter-coated, and MWCNT dispersions were spin-coated on top of the gold electrodes. The devices were then annealed under vacuum at 150 °C for 5 min. The typical thickness of the MWCNT films is in the range of 30-60 nm measured with a profiler. The typical resistance for the MWCNT films is in the range of 0.2-0.5 M Ω .

Device measurement.

We investigated the sensory response by measuring the relative conductance change ($-\Delta G / G_0$) of the sensors upon exposure to the 20 VOCs (3 trials each). The current was recorded between the two electrodes under a constant bias voltage (0.05 V) from which the conductance change was calculated. Our sensor response is taken one at a time, under the same experimental conditions such as sensor exposure and refreshing time, analyte concentration, temperature, environmental humidity, *etc.*

12 References and Notes

- (1) Buszewski, B.; Kęsy, M.; Ligor, T.; Amann, A. *Biomed. Chromatogr.* **2007**, *21*, 553-566.
- (2) O'Neill, H. J.; Gordon, S. M.; O'Neill, M. H.; Gibbons, R. D.; Szidon, J. P. *Clin. Chem* **1988**, *34*, 1613-1618.
- (3) Phillips, M.; Gleeson, K.; Hughes, J. M. B.; Greenberg, J.; Cataneo, R. N.; Baker, L.; McVay, W. P. *Lancet* **1999**, *353*, 1930-1933.
- (4) Deng, C.; Zhang, J.; Yu, X.; Zhang, W.; Zhang, X. *J. Chromatogr. B* **2004**, *810*, 269-275.
- (5) Miekisch, W.; Schubert, J. K.; Noeldge-Schomburg, G. F. E. *Clin. Chim. Acta* **2004**, *347*, 25-39.
- (6) Stone, B.; Besse, T.; Duane, W.; Dean Evans, C.; DeMaster, E. *Lipids* **1993**, *28*, 705-708.
- (7) Di Francesco, F.; Fuoco, R.; Trivella, M.; Ceccarini, A. *Microchem. J.* **2005**, *79*, 405-410.
- (8) Libardoni, M.; Stevens, P.; Waite, J. H.; Sacks, R. *J. Chromatogr. B* **2006**, *842*, 13-21.
- (9) Amann, A.; Smith, D. *Breath Analysis for Clinical Diagnosis And Therapeutic Monitoring*; World Scientific Publishing Company, 2005.
- (10) Allen, B. L.; Kichambare, P.; Star, A. *Adv. Mater.* **2007**, *19*, 1439-1451.
- (11) Kauffman, D. R.; Star, A. *Angew. Chem. Int. Ed.* **2008**, *47*, 6550-6570.
- (12) Kim, S. N.; Rusling, J.; Papadimitrakopoulos, F. *Adv. Mater.* **2007**, *19*, 3214-3228.
- (13) Snow, E. S.; Perkins, F. K.; Robinson, J. A. *Chem. Soc. Rev.* **2006**, *35*, 790-798.
- (14) Peng, G.; Trock, E.; Haick, H. *Nano Lett.* **2008**, *8*, 3631-3635.

- 1
2
3
4 (15) Peng, G.; Tisch, U.; Haick, H. *Nano Lett.* **2009**, *9*, 1362-1368.
5
6 (16) Star, A.; Han, T.; Joshi, V.; Gabriel, J.; Grüner, G. *Adv. Mater.* **2004**, *16*, 2049-2052.
7
8 (17) Someya, T.; Small, J.; Kim, P.; Nuckolls, C.; Yardley, J. T. *Nano Lett.* **2003**, *3*, 877-
9 881.
10
11
12 (18) Salehi-Khojin, A.; Khalili-Araghi, F.; Kuroda, M. A.; Lin, K. Y.; Leburton, J.; Masel,
13 R. I. *ACS Nano* **2011**, *5*, 153-158.
14
15 (19) Gomez-Navarro, C.; Pablo, P. J. D.; Gomez-Herrero, J.; Biel, B.; Garcia-Vidal, F. J.;
16 Rubio, A.; Flores, F. *Nat Mater* **2005**, *4*, 534-539.
17
18 (20) Muñoz, B. C.; Steinthal, G.; Sunshine, S. *Sensor Review* **1999**, *19*, 300-305.
19
20 (21) Lonergan, M. C.; Severin, E. J.; Doleman, B. J.; Beaber, S. A.; Grubbs, R. H.; Lewis, N.
21 S. *Chemistry of Materials* **1996**, *8*, 2298-2312.
22
23 (22) Huang, J. *Adv. Polym. Technol.* **2002**, *21*, 299-313.
24
25 (23) Zhang, W.; Swager, T. M. *J. Am. Chem. Soc.* **2007**, *129*, 7714-7715.
26
27 (24) Zhang, W.; Sprafke, J. K.; Ma, M.; Tsui, E. Y.; Sydlik, S. A.; Rutledge, G. C.; Swager,
28 T. M. *J. Am. Chem. Soc.* **2009**, *131*, 8446-8454.
29
30 (25) Albert, K. J.; Lewis, N. S.; Schauer, C. L.; Sotzing, G. A.; Stitzel, S. E.; Vaid, T. P.;
31 Walt, D. R. *Chem. Rev.* **2000**, *100*, 2595-2626.
32
33 (26) Lim, S. H.; Feng, L.; Kemling, J. W.; Musto, C. J.; Suslick, K. S. *Nat. Chem.* **2009**, *1*,
34 562-567.
35
36 (27) Yaws, C. L. *Yaws Handbook of Vapor Pressure: Antoine Coefficients*; Gulf Publishing
37 Company, 2007.
38
39 (28) Balasubramanian, K.; Burghard, M. *Small* **2005**, *1*, 180-192.
40
41
42
43
44
45
46
47
48
49
50
51
52
53
54
55
56
57
58
59
60

- 1
2
3 (29) Kim, W.; Javey, A.; Vermesh, O.; Wang, Q.; Li, Y.; Dai, H. *Nano Lett.* **2003**, *3*, 193-
4 198.
5
6
7
8 (30) Zahab, A.; Spina, L.; Poncharal, P.; Marlière, C. *Phys. Rev. B* **2000**, *62*, 10000.
9
10 (31) Grate, J. W. *Chem. Rev.* **2000**, *100*, 2627-2648.
11
12 (32) Grate, J. W.; Abraham, M. H. *Sens. Actuators B* **1991**, *3*, 85-111.
13
14 (33) Grate, J. W. *Chem. Rev.* **2008**, *108*, 726-745.
15
16 (34) Kolb, H. C.; Finn, M. G.; Sharpless, K. B. *Angew. Chem. Int. Ed.* **2001**, *40*, 2004-2021.
17
18 (35) Dondoni, A. *Angew. Chem. Int. Ed.* **2008**, *47*, 8995-8997.
19
20 (36) Chatterjee, A. K.; Choi, T.; Sanders, D. P.; Grubbs, R. H. *J. Am. Chem. Soc.* **2003**, *125*,
21 11360-11370.
22
23 (37) Trnka, T. M.; Grubbs, R. H. *Acc. Chem. Res.* **2001**, *34*, 18-29.
24
25 (38) Becer, C.; Hoogenboom, R.; Schubert, U. *Angew. Chem. Int. Ed.* **2009**, *48*, 4900-4908.
26
27 (39) Osswald, S.; Havel, M.; Gogotsi, Y. *J. Raman Spectrosc.* **2007**, *38*, 728-736.
28
29 (40) Amer, M. *Raman Spectroscopy, Fullerenes and Nanotechnology*; Royal Society of
30 Chemistry, 2010.
31
32 (41) Antunes, E.; Lobo, A.; Corat, E.; Trava-Airoldi, V.; Martin, A.; Veríssimo, C. *Carbon*
33 **2006**, *44*, 2202-2211.
34
35 (42) Mennella, V.; Monaco, G.; Colangeli, L.; Bussoletti, E. *Carbon* **1995**, *33*, 115-121.
36
37 (43) Crews, P.; Jaspars, M.; Rodríguez, J. *Organic Structure Analysis*; Oxford University
38 Press, 2009.
39
40 (44) Jurs, P. C.; Bakken, G. A.; McClelland, H. E. *Chem. Rev.* **2000**, *100*, 2649-2678.
41
42 (45) Kang, Y.; Rudkevich, D. M. *Tetrahedron* **2004**, *60*, 11219-11225.
43
44
45
46
47
48
49
50
51
52
53
54
55
56
57
58
59
60